Investigation of Spatial Structure Development of the Hardened C_3S Pastes by Serial Block-Face SEM

Fei Yang[1], Xianping Liu[1,2,*], Shunfeng Wang[1], Peiming Wang[1,2], Ian Robinson[1,3], Bo Chen[1,2,3,*]

[1]School of Materials Science and Engineering, Tongji University, Shanghai 201804, China

[2]Key Laboratory of Advanced Civil Engineering Materials (Tongji University), Ministry of Education, Shanghai 201804, China

[3]London Centre for Nanotechnology, University College London, London WC1H 0AH, U.K.

* Correspondence authors:

lxp@tongji.edu.cn (X.L.) and bo.chen@tongji.edu.cn (B.C.); Tel.: +86-21-39526230

ABSTRACT

Hardened tricalcium silicate (C_3S) pastes cured for different times from 12 hours to 28 days were studied by serial block-face scanning electron microscopy (SBFSEM) and their spatial structures were quantitatively analyzed. SBFSEM allows three-dimensional (3D) structural images of the specimens to be acquired with a pixel size down to 16.6 nm × 16.6 nm. From these 3D images, the morphological characteristics of different components of the hardened C_3S pastes in three-dimensions can be observed directly, such as the connected pores and closed pores. Moreover, the degree of hydration and porosity of the measured samples can also be estimated as well. The hydration degree and porosity calculated through results from SBFSEM measurements were compared with results from traditional TG-DSC, X-ray CT and MIP, and it proves that SBFSEM has good applicability in the field of cement-based materials.

Keywords: serial block-face scanning electron microscopy (SBFSEM), C_3S pastes, three-dimensional imaging, degree of hydration, porosity

1. Introduction

Tricalcium silicate (C_3S) is the most important constituent of normal Portland cement clinkers and accounts for about 50% - 70% of its weight [1]. The main hydrates produced by normal Portland cement hydration for strength development are hydrated calcium silicate (C-S-H) and calcium hydroxide (CH), both of them are generated mostly by the reaction of C_3S with water [2]. The structure and hydrates of C_3S are relatively simple compared with those of normal Portland cement, therefore C_3S is often used instead of normal Portland cement for studying the hydration process [3, 4]. Since the hydration process determines the early characteristics of the cement mortar and concrete, such as strength development and durability, it has been studied for decades. Therefore, progress made in understanding the microstructure development during cement hydration process will attract wide attention, and could help researchers to manipulate the process, hence improving the quality and cost of the cement mortar and concrete [5-7]. However, so far, the mechanism of cement hydration has not yet been fully understood. The microstructure characterization, especially the characterization of pore structure evolution, has not been able to obtain solid results because the limitations of mainstream measurement methods. In fact, currently, due to the lack of sufficient experimental observation and data analysis, especially the direct observations that could be used to guide the numerical simulation of microstructure and its development, even the mechanism of early

cement hydration has not yet reached consensus [8-11].

Thermal analysis (TA), quantitative X-ray diffraction (QXRD), mercury intrusion porosimetry (MIP), nitrogen adsorption, small angle scattering (SAS) by X-rays or neutrons, backscattered electron image analysis (BSE-IA) and X-ray computed tomography (CT) have been used to study the cement hydration and their microstructure development, notably to characterize the pore structure. Among those techniques, TA and QXRD are often used to identify phases and study the hydration degree of cement pastes [7, 12]. MIP can measure and analyze most of the pores from the nanometer to the micrometer level [13]. The nitrogen adsorption method is mainly used to analyze the nano-scale pores [14]. Considering the scale factor, most of the gel pores and gel particles are mainly characterized by SAS [15]. BSE-IA performs statistical analysis on two-dimensional (2D) BSE micrographs, thereby could calculate the hydration degree and pores of cement-based materials [16]. X-ray CT can perform three-dimensional (3D) structure reconstruction of samples based on the acquired 2D projections [17]. While each technique has its advantages and disadvantages. For example, MIP, nitrogen adsorption and SAS can be used to study pores of different sizes, but these all are indirect measurement methods and they are not able to characterize the porosity heterogeneity along the altered profile. BSE-IA can be used to calculate the hydration degree and analyze pore structure from the directly obtained images, but this is limited to two dimensions. Compared with other traditional methods, 3D visualization techniques have great advantages in revealing the real spatial distribution and irregular morphology of the hardened cement pastes. X-ray CT can acquire 3D spatial images of samples and has been used in the field of studying cement-based materials in the last a couple of decades [18, 19]. Although its applications in the field are gradually being promoted, so far, qualitative and quantitative research on cement-based materials using X-ray CT is still not much.

Like X-ray CT, serial block-face scanning electron microscopy (SBFSEM) [20] is a 3D imaging technology originally designed for life science research, which has been gradually extended to other research fields. It is becoming one of the key methods for acquiring 3D images of biological materials [21], polymer materials [22], composite materials and metal alloys [23-25]. From these results, the internal features of the measured materials can be observed and analyzed quantitatively. For SBFSEM measurements, materials are usually embedded in epoxy resin first, which can effectively avoid the collapse of their 3D structure when imaging in the vacuum environment of the electron microscopes. The embedded sample block is alternately cut by the built-in ultra-microtome and then imaged. The thickness of the slices in the Z-axis direction can reach 5 nm to 200 nm. The resolution of image slices in the XY plane can be as high as 1-2 nm, depends on the sample and the used electron microscope. Every time the sample is cut, the newly exposed surface is imaged by using back-scattered electron signals, and then a new cut will be performed again. This process is automatically performed continuously according to the set parameters [26, 27]. The 3D image is then obtained by stacking the serial slice images together. Compared with traditional serial-section imaging methods, SBFSEM has the images automatically registered and in sequence.

SBFSEM was used to study the hydration of C_3S with the water to cement (w/c) ratio of 0.6 in this work. Under BSE imaging, the gray-scale levels of unhydrated regions of the raw C_3S, hydrates and pores in the hardened C_3S pastes are all different [28]. Based on the resulting gray-scale levels of the slice images, Avizo and ImageJ software can be used to perform segmentation, 3D rendering and analysis on hundreds of slices obtained by SBFSEM [29]. For example, the size distribution and the connectivity of the pores can be observed, and the measured volume fractions of the

unhydrated C_3S can also be calculated directly. The changes in hydration degree and the shape of pores with time during the hydration of C_3S can also be analyzed in three dimensions. In this research, the hydration degree and pore structure of the hardened C_3S paste hydrated for 7 days was studied by SBFSEM first. The result was compared with those obtained by the traditional methods such as thermogravimetric-differential scanning calorimetry (TG-DSC), MIP and X-ray CT to verify the applicability of the technique. Finally, the 3D technique, SBFSEM was used to study the evolution of hydration degree and pore structure of the hardened C_3S pastes after various hydration ages including 12 hours, 3 days, 7 days and 28 days.

2. Materials and methods

2.1 Raw materials and the sample preparation

C_3S used in the work was provided by DMT Materials Technology Co., Ltd. A secondary electron micrograph is presented in Fig. 1a. The morphology of the C_3S particles looks regular, and the specific area measured by the Brunauer-Emmett-Teller (BET) method is 1.8212 ± 0.0028 m^2/g. According to the particle size distribution chart in Fig. 1b, obtained from a laser particle analyzer, it can be seen that most of the C_3S particles have a particle size of between 1 μm and 6 μm. In order to evaluate the purity of the received C_3S specimen, 10% of Al_2O_3 by weight was used as a standard reference mixer in C_3S. TOPAS V4.2 was used to refine the XRD pattern of the Al_2O_3 mixed C_3S sample, the Rietveld refinement result showed that the raw material contained 97.8% of C_3S and 2.2% of β-C_2S (Fig. 2).

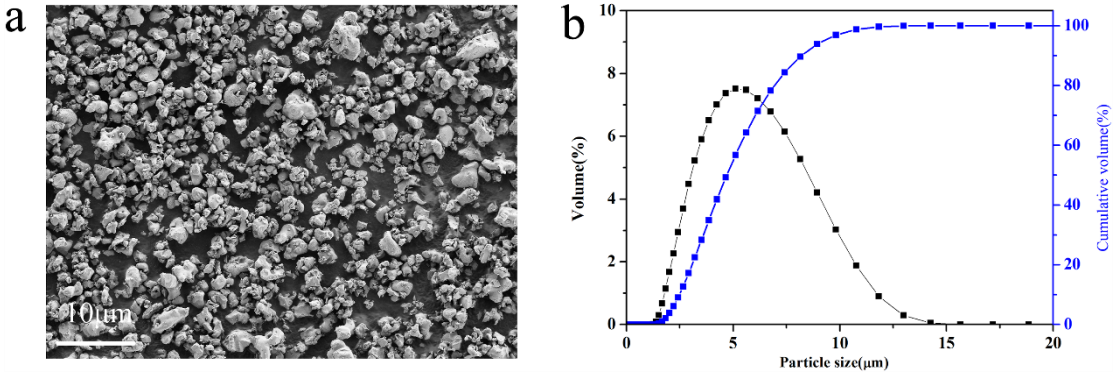

Fig. 1. Characterization of the raw C_3S specimen. (a) Secondary electron micrograph of the C_3S; (b) Size distribution of the C_3S particles.

Since the C_3S particles are ultra-fine powders, in order to ensure that the mixed paste has better homogeneity, the w/c ratio was selected to be 0.6 in this experiment. The C_3S particles were mixed with deionized water and stirred quickly with a glass rod for about 3 minutes. The evenly mixed paste was poured into a plastic vessel, then sealed to prevent carbonization and left to cure for 12 hours, 3 days, 7 days and 28 days at temperature of 20 ± 2°C. The cured samples at predetermined ages were broken into pieces and stopped hydration by immersed in the ethanol for 1day and then dried at 40 ± 2℃ in an oven. These prepared samples were then kept for further measurements.

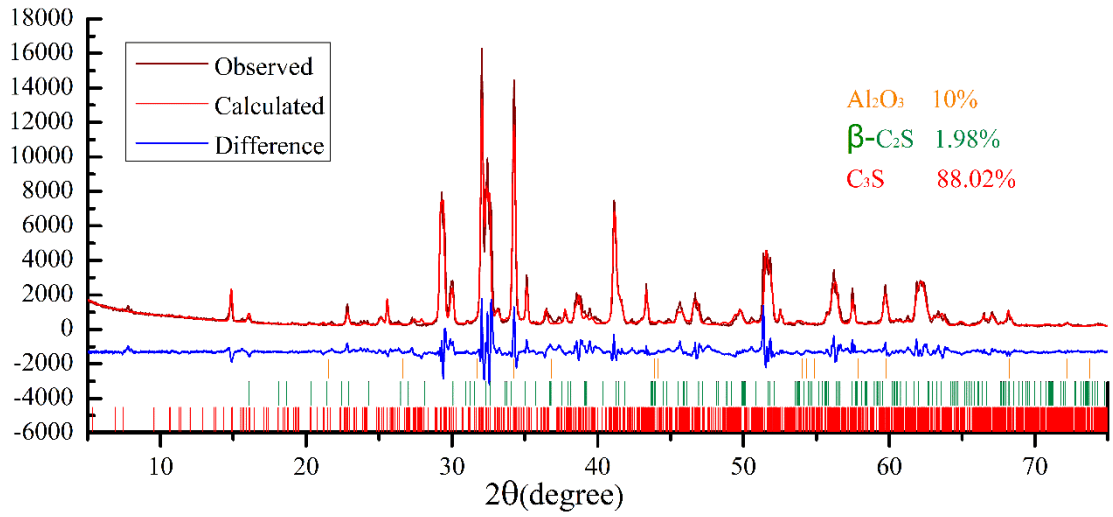

Fig. 2. The result of Rietveld refinement for the mixed C_3S specimen with 10% Al_2O_3 as a standard reference mixer.

For measurements by SBFSEM, the cured C_3S paste needs to be embedded in the epoxy resin in advance. The epoxy resin used in this experiment is Agar 100 resin supplied by Agar Scientific Ltd. The embedding was performed under vacuum condition, and then placed at room temperature (20°C) for 30 minutes, further cured at 60°C for about 48 hours. The epoxy resin embedding method has two advantages: it avoids carbonization of the C_3S paste, and also improves the sample stability for imaging in vacuum. A Leica EM UC7 microtome was used to trim the embedded sample into a pyramid shape, and then a total depth of about 5 μm of the sample was cut by a glass knife to ensure that the upper surface of the sample to be measured by SBFSEM is flat. Finally, conductive silver paste was applied around the pyramid-like sample to help to prevent charging on the sample surface during SBFSEM measurement.

2.2 Methods

The morphology of the raw material, the C_3S particles, was observed by an SEM (Zeiss Sigma 300VP, Carl Zeiss Microscopy GmbH) and the size distribution of the particles was measured by a laser particle size analyzer (LS230, Beckman Coulter Ltd.). The dispersion liquid used during the measurement was ethanol.

The specific surface area of the C_3S specimen was calculated by using the absorption data via the Brunauer-Emmett-Teller (BET) method, using a Quadrachrome absorption instrument (Autosorb-iQ3, Quantachrome).

Powder X-ray Diffraction (XRD) measurement of the C_3S specimens was performed by a Rigaku D/max 2550 VB3+/PC diffractometer (Rigaku International Corporation) using Cu Kα radiation at 40 kV and 250 mA, with 2θ from 5° to 75°. The raw C_3S particle mixture (with Al_2O_3) was measured by stepping scanning with a step of 0.02° with 2 s exposure time. The cured hardened C_3S pastes were ground into very fine powders first and then measured using continuous scanning with 5°/min speed.

An X-ray micro-CT, Nano Voxel 3000 (Sanying Precision Instruments Co., Ltd), was used to do the tomographic scan of the hardened C_3S paste cured for 7 days. The sample was trimmed to a needle-like shape, about 500 μm in diameter. The X-ray tomographic scan was operated at 90 kV and 20 mA with an angle step of 0.2° from −180° to 180° (totally 1801 projections were acquired)

with 3 s exposure time per projection. The total time for the scan was about 3 hours. The pixel size of the reconstructed tomogram slices is 700 nm × 700 nm.

An MIP instrument (Auto pore IV9500 V1.09, Micromeritics Instrument Corp.) was used to measure the pore size distribution of the sample. The penetration pressure was set from 0.1 psi to 20,000 psi. The diameter of the measured sample needs to be made between 3 mm and 5 mm to ensure the accuracy of the obtained results.

The TG-DSC curves were acquired by an SDT Q600 analyzer (TA Instrument, USA) at heating rate of 10℃/min in N_2 flow at a rate of 60 mL/min. CH decomposition was calculated according to the TG test. The TG-DSC result was used to calculate the CH content quantitatively.

The SBFSEM system used in this work consists of an SEM (Zeiss Sigma 300VP, Carl Zeiss Microscopy GmbH) and a commercial 3View unit (Gatan UK) [20, 30, 31]. The BSE signal was selected to image the sample in order to show different components in the samples with different gray-scale levels. The 3View unit, a built-in ultra-microtome system of the SBFSEM, performs continuous cutting and BSE imaging according to the set parameters. That is, after each automatic cutting, the freshly exposed surface of the sample is imaged by the BSE detector. This serial cutting and imaging continues until hundreds or thousands of BSE micrographs are acquired upon request. Further details of the operating procedures can be found in other work [32].

In this study, the cutting thickness of each slice and cutting speed of the ultra-microtome were set to be 20 nm and 0.6 mm/s, respectively. The dwell time of the BSE detector was 1.5 μs and the pixel size of the acquired BSE images is 16.6 nm × 16.6 nm. Under such parameter setting, a data set consisting of 900 slices are collected in about 8 hours.

2.3 Data processing

Preprocessing of the data set was performed by ImageJ [33] before segmentation of the 3D images, and then segmentation and quantitative analysis were done by Avizo [29, 30]. According to the experience of BSE imaging of cement materials [16, 28]: pores, hydrates and unhydrated C_3S of raw materials are presented with different gray-scale levels within the acquired BSE images. The tangent method is used to make a preliminary determination of the threshold gray-scale level for different components in the specimens, which provides a basis for subsequent threshold segmentation by Avizo. The processing of a large number of complex data requires a high-performance computer with Avizo software. Data processing by Avizo mainly includes the following steps: alignment, noise reduction, segmentation, rendering and visualization and volume analysis. The main data processing flow is shown in Fig. 3.

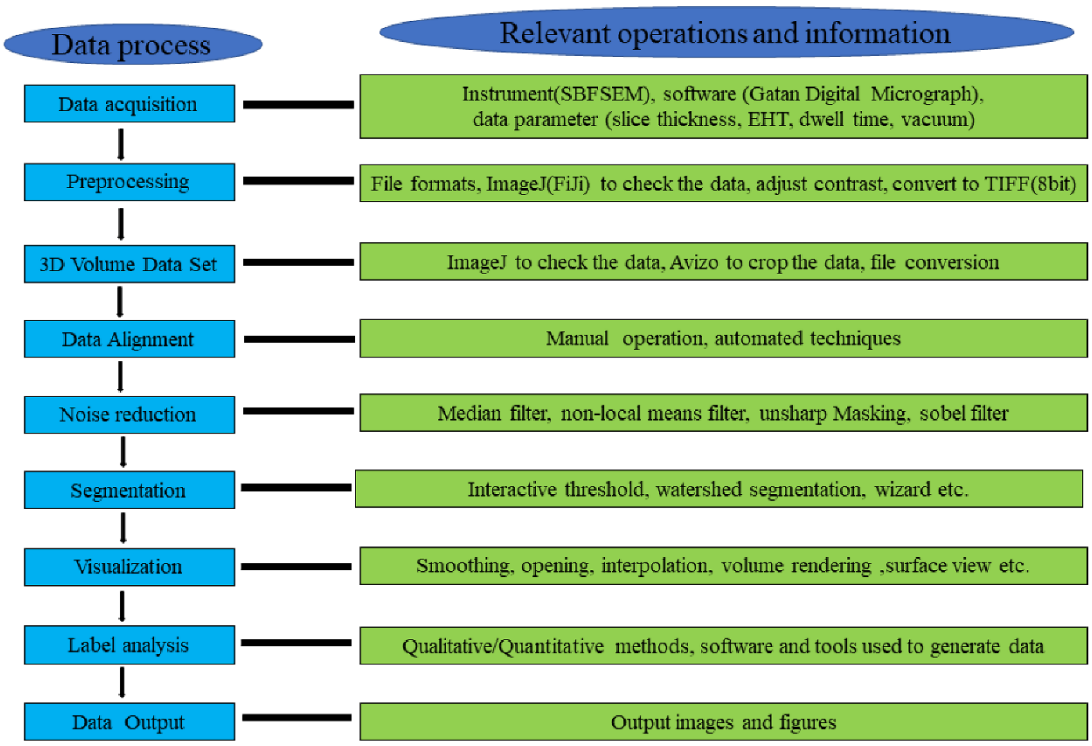

Fig. 3. Main steps and operation in SBFSEM data acquisition and processing

3. Results and discussion

3.1 Analysis of the hardened C_3S paste hydrated for 7 days

Fig. 4a is the BSE image of the cross-section of the whole mounted sample at lower magnification. The gray part in the middle is identified as the hardened C_3S paste (labelled by red arrow), the large black region surrounding it is the epoxy resin, and the regions with white dots around the edges of the epoxy resin is the conductive silver paste. Only the central part of the sample, i.e. the hardened C_3S paste, was chosen for high-resolution imaging. Fig. 4b shows the first acquired two-dimensional (2D) BSE image of the serial slices of the hardened C_3S paste after 7 days of hydration. The generated pixel size of the image is 16.6 nm × 16.6 nm. The black parts in Fig. 4b represent the pores, the large gray part is the hydrates, and the whiter parts are unhydrated C_3S particles of the raw materials. Fig. 4c shows the 100th, 300th, 500th and 700th images in the serial of slice images obtained by SBFSEM, the changes at the corresponding positions in different images can also be clearly seen.

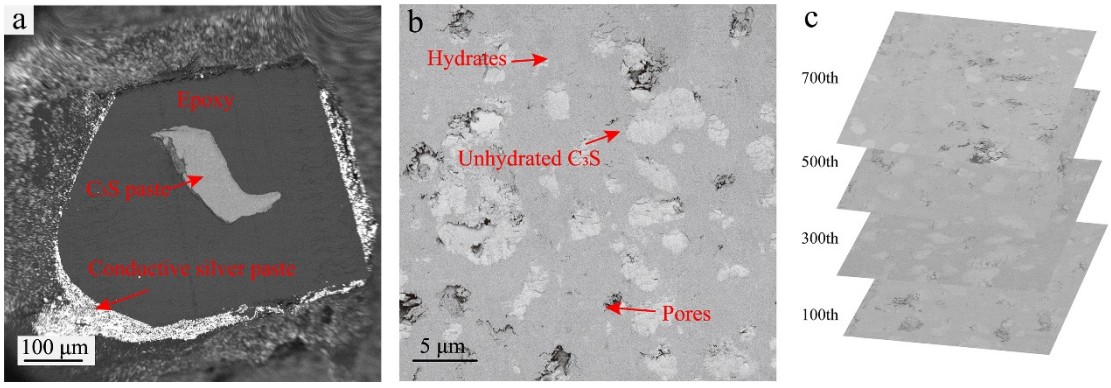

Fig. 4. Two-dimensional (2D) slice images of the sample from SBFSEM measurement. (a) BSE micrograph of the whole sample. (b) The first acquired 2D image of the serial slices of the hardened C_3S paste after 7 days of hydration. (c) The 100th, 300th, 500th and 700th images of the serial slice images.

Fig. 5a shows the 3D rendered volume image of the C_3S paste after 7 days of hydration. Fig.s 5b&c present the distribution of the unhydrated C_3S and the pores within the specimen, respectively. In these 3D structural images, the blue parts represent the unhydrated C_3S particles, the red and yellow parts represent the pores and the gray regions are the hydrates. The distribution of the hydrates, the pores and the unhydrated C_3S particles in three dimensions can be seen clearly. The 3D pore network, the tortuosity and connectivity can also be viewed clearly. From these segmented 3D images, the porosity of the measured specimens can be calculated using Avizo software. The porosity is defined as the ratio of the total volume of pores to the total volume of the measured specimen. Since the connected pores have an important effect on the permeability of cement-based materials, the classification of the connected pores and the closed pores have been done using Avizo software. The connected pores (yellow parts in Fig. 5) are defined as the pores connected to any boundary of the considered volume. The closed pores (red parts in Fig. 5) are defined as the pores that has no contact with any face of the considered volume. The use of the imaged volume to define the sample boundaries is a kind of subjective and may overcount the connected pores for a real sample. This point is addressed below.

Since the size of the 3D rendered volume image is 18 μm × 33 μm × 33 μm, the total calculated volume of the pores is 2744 μm^3, so the porosity of the measured sample hydrated for 7 days is 14.1%. The connected pores and the closed pores count 6.2% and 7.9%. Based on the 3D analysis, the degree of hydration at time t can be calculated according to the following equations [34, 35], which results in 81.3% at 7 days of hydration.

$$\alpha_t(\%) = \{1 - \frac{V(t)}{V(0)}\} \times 100\% \quad (1)$$

$$\mathrm{V(0)(\%)} = \frac{1}{1+\rho_c \times (m_w/m_c)} \times 100\% \quad (2)$$

In the equations 1 and 2, α_t presents the degree of hydration of the C_3S; V(t) presents the volume of the unhydrated C_3S at the hydration time t, this value can be derived from the 3D analysis of the volume images (0.066). V(0) presents the volume of the C_3S before hydration (0.349); ρ_c presents the specific gravity of C_3S, (3.1, measured by helium pycnometry); m_w/m_c =0.6 (w/c ratio).

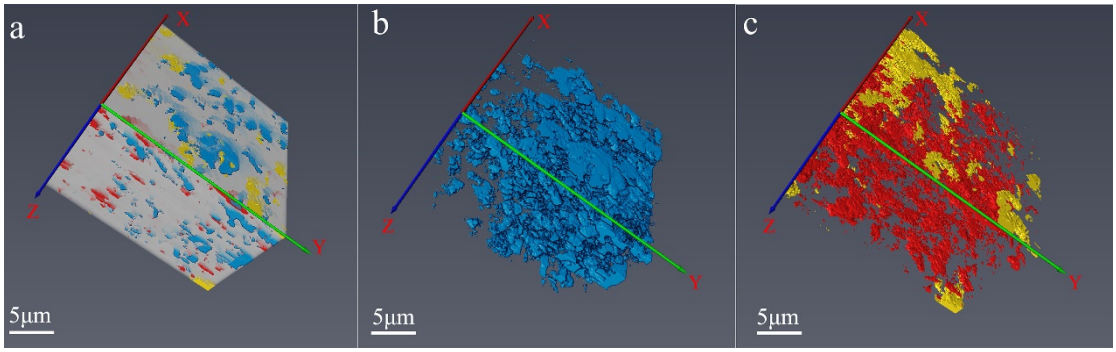

Fig. 5 3D rendering images of the C_3S hydrated for 7days from SBFSEM measurement. (a) 3D image of the hardened C_3S paste. (b) 3D image of the unhydrated parts of the C_3S particles in the specimen. (c) 3D image of the connected pores (yellow parts) and closed pores (red parts) within the specimen.

In order to minimize the edge effects and reduce the time of data processing, the analyzed target sample volumes in this study were chosen from the center region of the embedded hardened C_3S paste, where the homogeneity of the pastes is also considered as the best. To verify whether the sampling is representative, the changes of the hydration degree and porosity of the samples as a function of the selected volumes are shown in Fig. 6. In Fig. 6b, it can be seen that once the selected sample volumes are larger than 1.4×10^4 μm^3, their hydration degrees tend to be stable, the porosity of the samples tends to be stable while the selected sample volumes are larger than 1.8×10^4 μm^3(Fig 6a). This confirms that the sample size (2.0×10^4 μm^3) chosen in this work is appropriate.

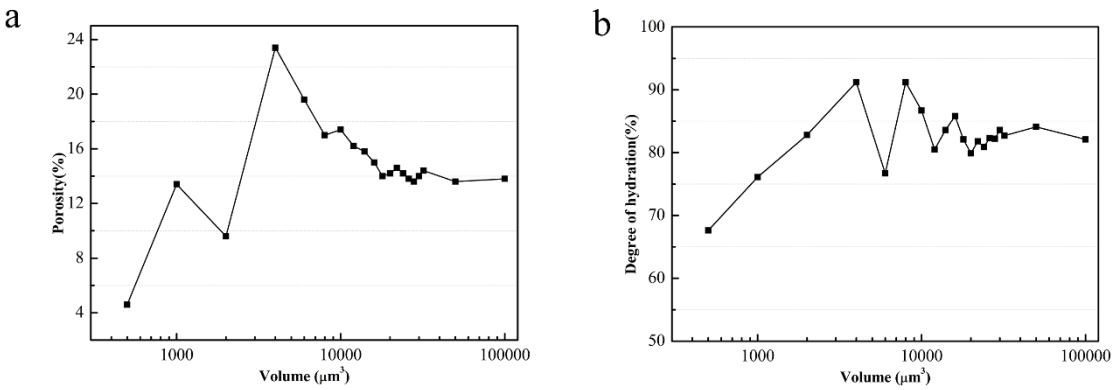

Fig.6 Changes in porosity and the degree of hydration against the volume changing. (a) Porosity of the selected samples and (b) The hydration degree of the selected samples with their volume increasing.

3.2 X-ray Computed Tomography (CT)

Fig. 7a shows one of the tomogram slices of the reconstructed sample volume from X-ray CT measurement of the C_3S paste hydrated for 7 days. A 532 μm × 532 μm square region (labelled in Fig. 7a) is selected for statistical analysis, in an attempt to avoid edge effects as well. Fig. 7b shows a 532 × 532 × 532 μm^3 volume with the gray regions representing the hydrated C_3S, the blue regions representing the unhydrated C_3S and the red and yellow parts representing the pores. The distribution of the unhydrated C_3S particles and the pores in three dimensions is shown in Fig.s 7c&d, the connected pores and the closed pores are shown in Fig. 7d in yellow and red, respectively. According to the method of calculating the degree of hydration and porosity above, the X-ray CT measurement gives the degree of hydration as 91.7%, the total porosity as 2.7%, in which the connected pores counts one third and the closed pores counts another two thirds. Compared with the analysis from the SBFSEM measurement, the results of the X-ray CT measurement showed that the degree of hydration increased by 12.8% and the total porosity decreased by 80.9%. This can be due to the much lower resolution of the used X-ray CT instrument which makes the smaller unhydrated particles and pores not be detected during the measurement.

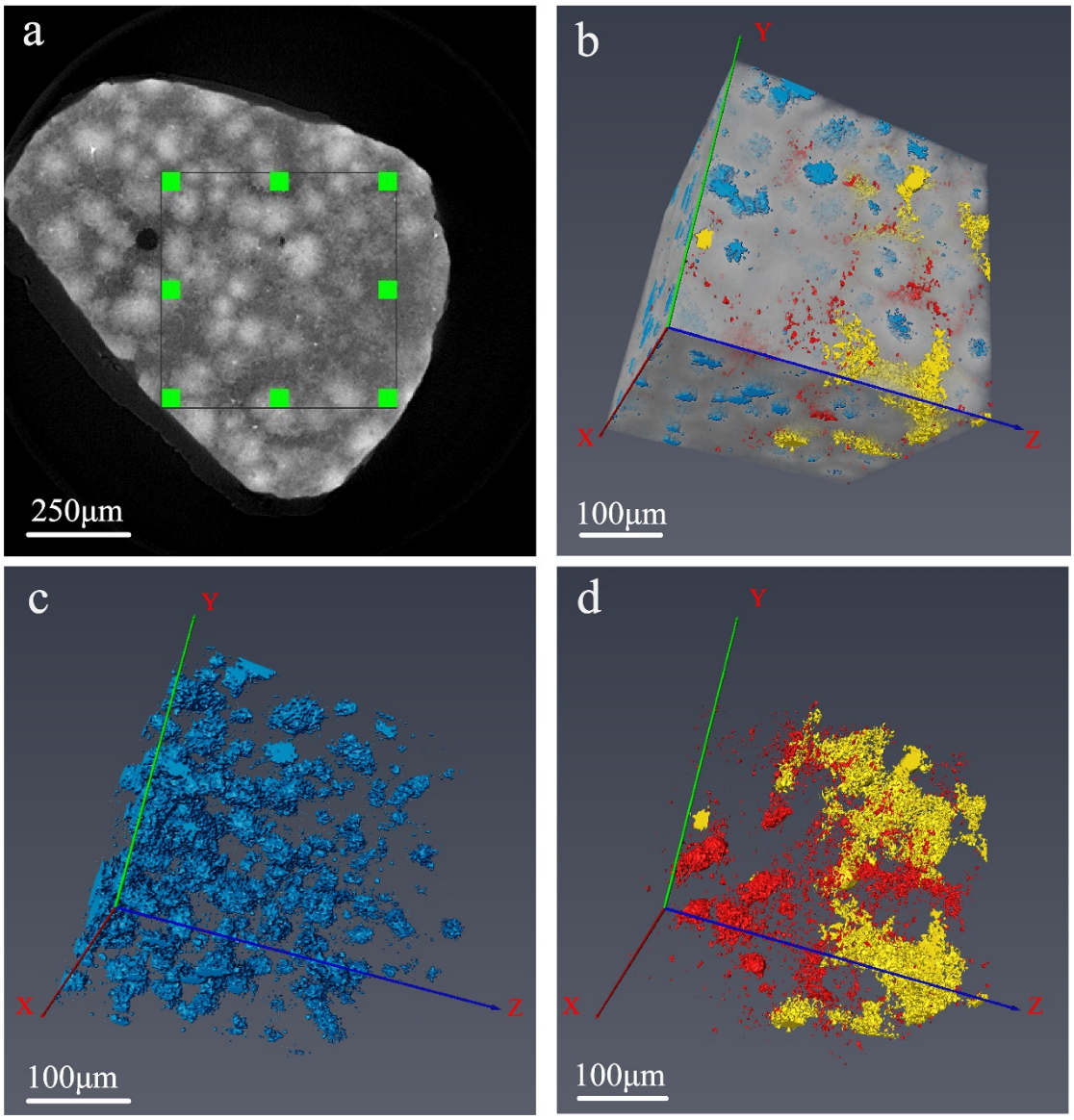

Fig. 7 Structural images of the C_3S paste hydrated for 7 days from X-ray CT measurement (a) A reconstructed tomogram slice image of the C_3S paste. (b) 3D reconstructed image of the C_3S paste. (b) the unhydrated C_3S particles. (c) the connected pores (yellow parts) and closed pores (red parts).

3.3 Differential Scanning Calorimetry (DSC)

The TG-DSC curves of hardened C_3S paste hydrated for 7 days and 360 days are shown in Fig. 8. The fully hydrated C_3S paste sample was aged for 360 days, which was prepared by breaking and grinding the already-hardened C_3S paste at the hydration age of 180 days, and then mixing with excess water for continual hydration. This sample aged for 360 days was measured by XRD. It can be seen that the raw C_3S has hydrated completely and there is only a small amount of carbonized material (Fig. 9), which may be produced during the grinding process. Calcium carbonate has an endothermic peak in TG-DSC measurements at about 700°C, which is not seen here in Fig. 8, so the slight carbonization phenomenon in this experiment is negligible.

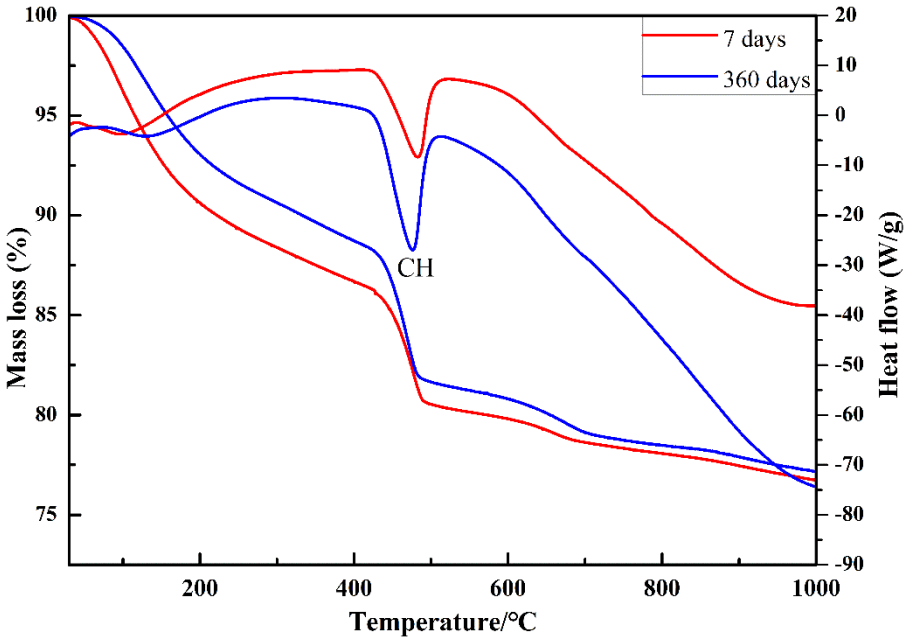

Fig. 8 The TG-DSC curves of the C_3S paste hydrated for 7days and 360 days

The degree of hydration of a cement paste is determined by the ratio of the generated CH content at time t to the CH content in its fully hydrated status [36, 37]. In these TG-DSC curves, the endothermic peak around 483 °C is the endothermic peak of the CH decomposition. According to the mass loss of CH during the TG-DSC measurements (about 483 °C), the content of CH can be calculated. The degree of hydration of the C_3S paste after 7 days of hydration calculated from this is 76.5%, which is slightly lower than the 81.3% obtained from the SBFSEM measurement, but close. This could be because, in the 3D image segmentation process, some of the unhydrated particles with sizes around 16.6 × 16.6 × 16.6 nm^3 (a voxel size of the acquired 3D image) were identified as the hydrates, which caused the degree of hydration to be higher.

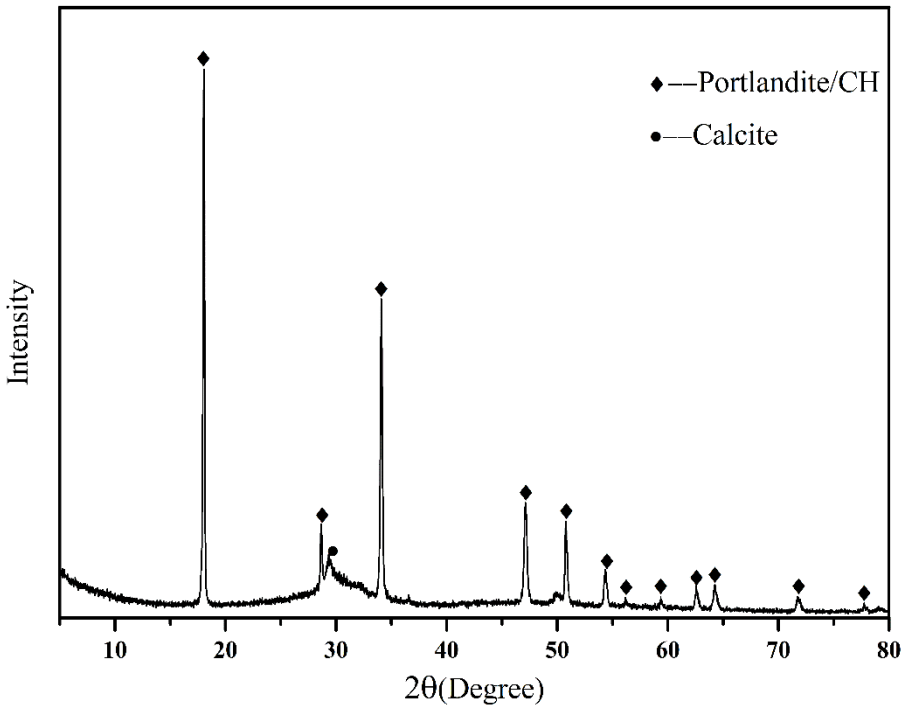

Fig. 9 The XRD pattern of the C_3S paste hydrated for 360 days.

3.4 Mercury Intrusion Porosimetry (MIP)

The pore size distribution of the sample after 7 days of hydration was measured by the MIP method as well, and the result is shown in Fig. 10. There are two distinct peaks around the sizes of 15 nm and 200 nm. The porosity obtained by MIP is shown in Table 1. Its total porosity is 21.4%. With reference to Wu's classification [38] of the pores of cement-based materials, the porosity obtained by the MIP and SBFSEM measurements was classified and compared. It should be noted that the two measurements were not performed using the same region of interest (ROI) of the same sample. Due to the intrinsic heterogeneity of the cement-based sample, the analytical data obtained by the two methods will have a certain extend of volatility. Pores smaller than 20nm were not identified by SBFSEM due to the cutting thickness of the sample. For pore diameters in the range of 20 nm - 50 nm, the values obtained by the SBFSEM measurement (2.4%) is in good agreement with the 2.3% obtained by MIP; for pore diameters in the range of 50 nm - 200 nm, the porosity measured by SBFSEM (6.2%) is slightly higher than the 5.4% porosity obtained by MIP. This supposes to be because MIP can only detect the connected pores, while SBFSEM measures both the connected and closed pores. For pores with diameters larger than 200 nm, the porosity of 5.5% obtained from SBFSEM is smaller than that from MIP (6.3%). The maximum pore diameter measured by the SBFSEM measurement is 7.7 μm, limited by the size of the measured sample. while the MIP measurement shows the largest pore is 10.4 μm. It is also possible that the high-pressure mercury intrusion causes the pores to be broken and enlarged during the measurement.

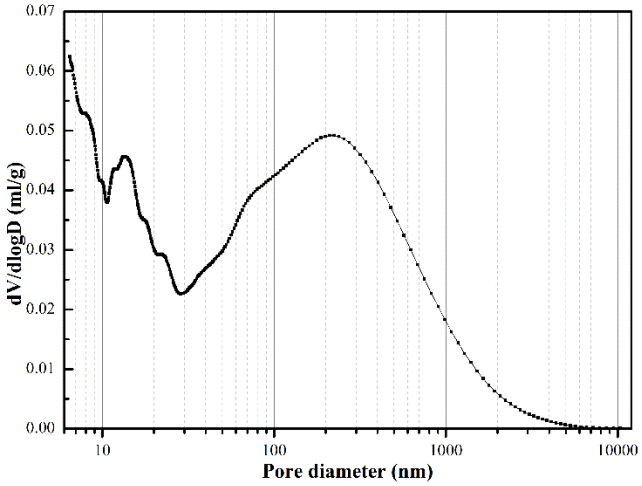

Fig. 10 Pore size distribution (dV/dlogD) of the C_3S paste hydrated for 7 days

The SBFSEM measurement can visualize both the tortuosity and connectivity of the pores in three dimensions and can also detect the closed pores. Generally, the statistical results presented here (in Table 1) show that SBFSEM measurement agrees well with the classical MIP method.

Table 1. Porosity measured by MIP and SBFSEM

Methods	Total porosity	Pore volume			
		<20 nm	20 nm–50 nm	50 nm–200 nm	>200 nm
MIP	21.4%	7.4%	2.3%	5.4%	6.3%
SBFSEM	14.1%	-	2.4%	6.2%	5.5%

3.5 Analysis of the hardened C_3S pastes hydrated for different times

The 3D SBFSEM analysis was repeatedly performed on the hardened C_3S pastes after 12 hours, 3 days and 28 days of hydration following the same analysis procedures. The 3D rendering results are shown in Fig. 11, in which the hydrates are rendered as gray, the unhydrated materials as blue and the pores as red and yellow. It can be seen that, as the hydration times increasing, the volumes of the unhydrated particles decrease. The volume fractions of the unhydrated materials calculated according to the equations 1 and 2, and the results are shown in Fig. 12. As can be seen from Fig. 12, the degree of hydration was 55.6% after 12 hours, while 88.8% of the C_3S has hydrated after 28 days.

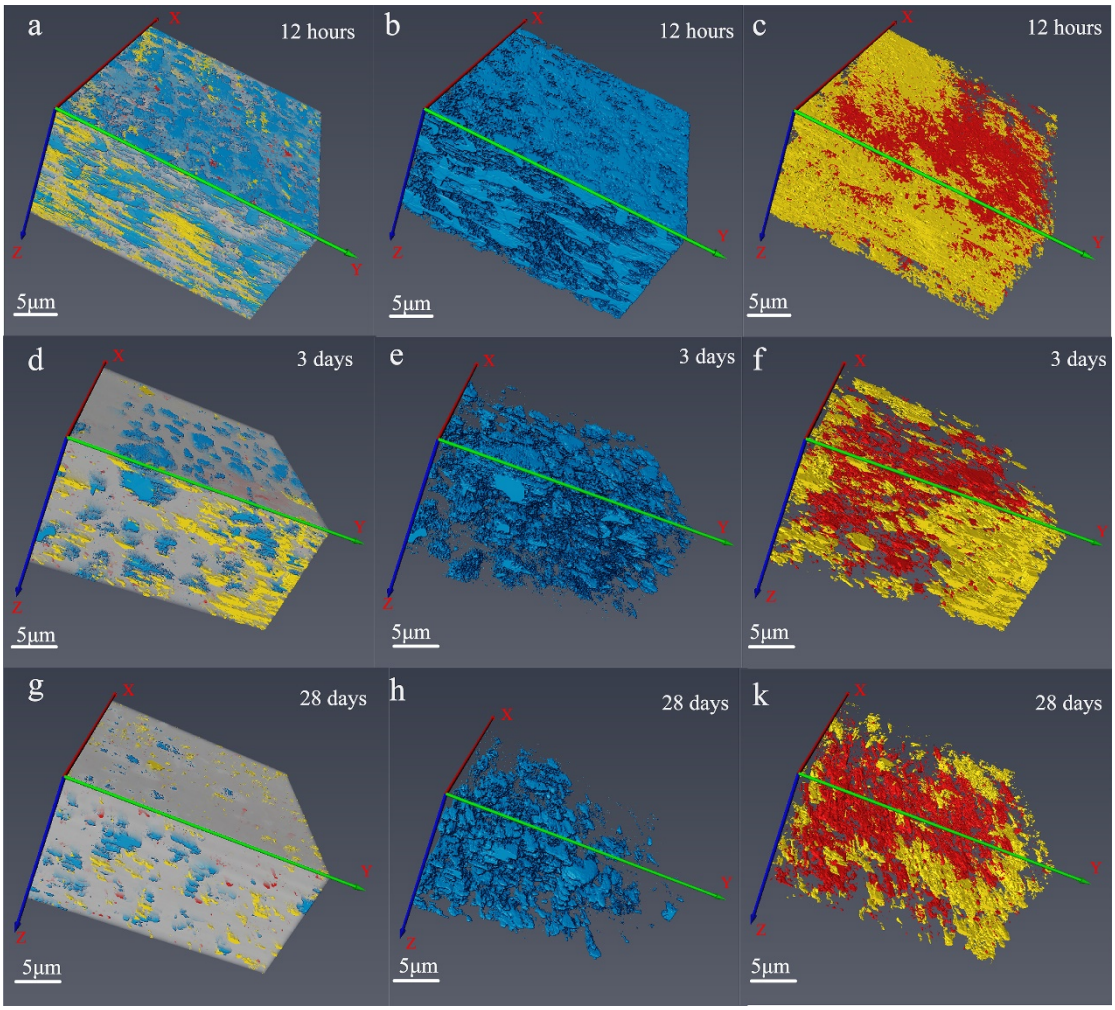

Fig. 11 3D structural images of the samples hydrated for different times. (a) the C_3S paste hydrated for 12 hours. (b) the unhydrated C_3S particles (blue) and (c) the connected pores (yellow) and the closed pores (red) of the C_3S paste hydrated for 12 hours. (d) the C_3S paste hydrated for 3 days. (e) the unhydrated C_3S particles and (f) the connected pores and the closed pores of the C_3S paste hydrated for 3 days. (g) the C_3S paste hydrated for 28 days. (h) the unhydrated C_3S particles and (k) the connected pores and the closed pores of the C_3S paste hydrated for 28 days.

From Fig.s 11c, 11f, 5c and 11k, it can be seen that the volumes of the connected pores (yellow) and all the pores show a decreasing trend with the increase of the hydration ages, while the volumes of the closed pores (red) do not change significantly. This indicates that, the volumes of the

connected pores decrease faster than the closed pores' while hydration is going on. The changes of the total porosity, the porosity fractions of the connected pores and the closed pores are shown in Fig. 13a. The volumes of the closed pores in the hardened C_3S pastes decrease very slow, much slower than that of the connected pores, hence that of all the pores as well. This is because most of hydration reactions happen on the surfaces or in the connected pores of the raw materials, while the hydration goes on and before the water starts to permeate into the closed pores, the produced solid hydration products would occupy the spaces in the connected pores and the open regions. This leads to the decrease of the volumes of the connected pores. Additionally, some of the connected pores would become the closed pores while hydration, this further decreases the volumes of the connected pores. On the other hand, the amount of water permeated into the closed pores is low and the process is time-consuming, at the same time there are new closed pores formed during hydration, this makes the volumes of the closed pores decrease slowly.

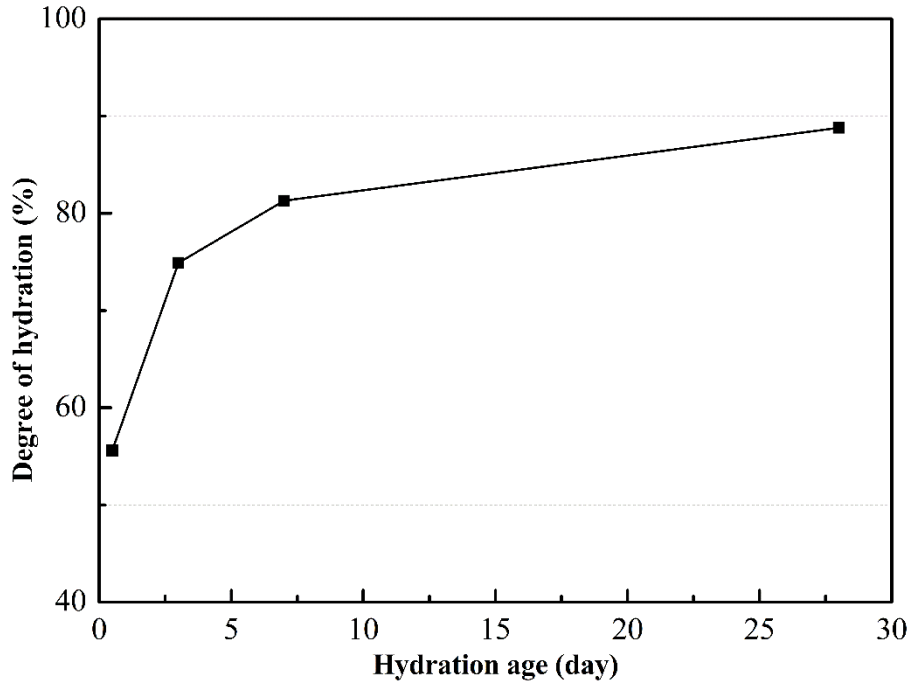

Fig. 12 The degree of hydration of the C_3S pastes with hydration of 12 hours, 3 days, 7 days and 28 days

Fig. 13b shows the porosity fractions of the pores with different sizes of the C_3S pastes hydrated for 12 hours, 3 days, 7 days and 28 days. It can be seen that the porosity fractions of the largest pores with diameters between 200 nm - 7700 nm decrease sharply during hydration, while smaller ones between 50 nm - 200 nm decrease much less, and the smallest ones between 20 nm - 50 nm stay almost unchanged. It demonstrates that with the continued hydration, hydrates fill in the pores and hence separate the large pores into smaller ones, which brings a finer pore structure and lower porosity in the hardened C_3S paste, that is, a denser hardened microstructure. On the other hand, the largest pores are almost all connected pores and the smallest pores are almost all close pores, the former group involve in the hydration reaction strongly and the latter group involve much less.

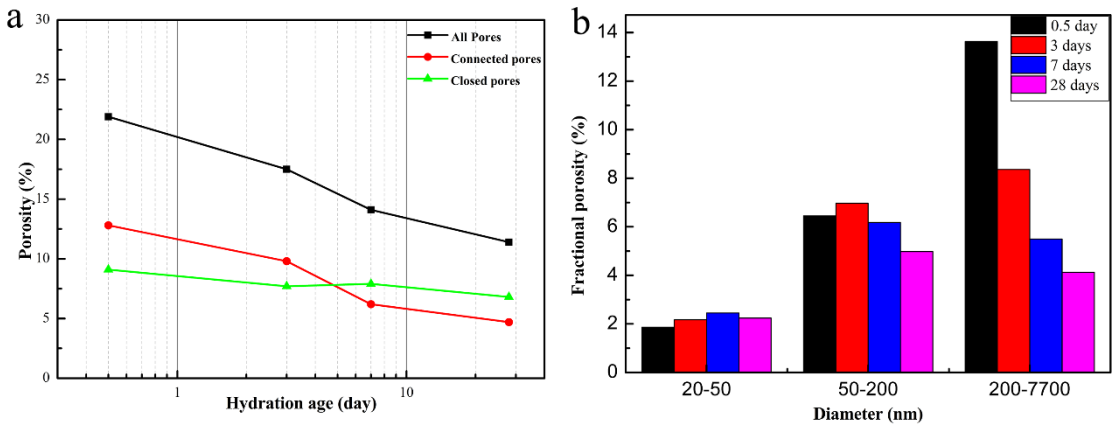

Fig.13 Changes of the porosity during hydration. (a)The changes of the total porosity, the porosity fractions of the connected and the closed pores during hydration. (b) The porosity fractions of the pores with different sizes of the C_3S pastes hydrated for 12 hours, 3 days, 7 days and 28 days.

4. Conclusions

In this work, the SBFSEM method is demonstrated to be a very promising technique for both imaging and quantitative study of the pore structure and chemical component identification of the hardened C_3S pastes during hydration. Applications of this technology on other cement-based materials can be performed in future.

This work studies the hydration degree and the pore structure of the hardened C_3S pastes in three dimensions, and observed their 3D structure through direct imaging at the nano-scale. Its main conclusions are:

(1) Embedding the hardened C_3S pastes into Agar 100 resin can not only avoid the carbonization of the hardened C_3S pastes, but also improves the stability of measurements of the hardened C_3S pastes during serial section imaging under high vacuum environment in SBFSEM.

(2) The spatial distribution of the unhydrated raw materials, the hydrates and the pores in the hardened C_3S pastes can be revealed directly with a voxel resolution of 16.6 nm in three dimensions. The degree of hydration based on the total volumes of the unhydrated raw materials can also be calculated. The higher the resolution of the acquired images, the smaller the difference. At the achieved spatial resolution in this work, there is a good agreement between the SBFSEM work and the classical TG-DSC results.

(3) The pore structure within the hydrated pastes can be presented clearly in three dimensions, by SBFSEM, to reveal the spatial tortuosity and connectivity information, and the pore diameter and porosity can also be quantitatively characterized by statistical analysis. Compared with X-ray CT, the resolution of the SBFSEM measurement is higher. Compared with the MIP method, SBFSEM can not only measure the connected pores but also the closed pores.

(4) With the increase of hydration time, the connected pores in hardened C_3S paste decrease much faster than the closed pores. The porosity fractions of the large pores between 200 nm -7700 nm decreases steadily during hydration, while those between 20 nm - 200 nm fluctuate, resulting in a denser hardened microstructure. These also indicate that the hydration reactions mostly happen in the connected pores and the open regions within the specimens.

Conflict of interest

The authors declare no conflict of financial interests.

Acknowledgements

This work was supported by the High-Level Talent Program "Materials Nano-structure" of Tongji University with grant No.s [152221] and [152243], the National Natural Science Foundation of China (Grant No. 51102181), the Joint Funds of the National Natural Science Foundation of China (Grant No. U1534207). B.C. thanks the support by the "Shanghai PuJiang Talent Program" with grant No. [18PJ1410400].

References

[1] K. Mei, X. Cheng, H. Zhang, Y. Yu, X. Gao, F. Zhao, J. Zhuang, X. Guo, The coupled reaction and crystal growth mechanism of tricalcium silicate (C_3S): An experimental study for carbon dioxide geo-sequestration wells, Constr. Build Mater. 187 (2018) 1286-1294.

[2] Q. Hu, M. Aboustait, T. Kim, M.T. Ley, J.W. Bullard, G. Scherer, J.C. Hanan, V. Rose, R. Winarski, J. Gelb, Direct Measurements of 3D Structure, Chemistry and Mass Density During the Induction Period of C_3S Hydration, Cem. Concr. Res. 89 (2016) 14-26.

[3] A. De La Torre, S. Bruque, J. Campo, M. Aranda, The superstructure of C_3S from synchrotron and neutron powder diffraction and its role in quantitative phase analyses, Cem. Concr. Res. 32(9) (2002) 1347-1356.

[4] L. Nicoleau, A. Nonat, A new view on the kinetics of tricalcium silicate hydration, Cem. Concr. Res. 86 (2016) 1-11.

[5] Y. Xi, D. Siemer, B. Scheetz, Strength development, hydration reaction and pore structure of autoclaved slag cement with added silica fume, Cem. Concr. Res. 27(1) (1997) 75-82.

[6] K.L. Scrivener, A. Nonat, Hydration of cementitious materials, present and future, Cem. Concr. Res. 41(7) (2011) 651-665.

[7] Y. Wei, W. Yao, X. Xing, M. Wu, Quantitative evaluation of hydrated cement modified by silica fume using QXRD, 27Al MAS NMR, TG–DSC and selective dissolution techniques, Constr. Build Mater. 36 (2012) 925-932.

[8] R. Cook, K. Hover, Mercury porosimetry of hardened cement pastes, Cem. Concr. Res. 29(6) (1999) 933-943.

[9] K.O. Kjellsen, H. Justnes, Revisiting the microstructure of hydrated tricalcium silicate—a comparison to Portland cement, Cem. Concr. Compos. 26(8) (2004) 947-956.

[10] J.E. Rossen, K.L. Scrivener, Optimization of SEM-EDS to determine the C–A–S–H composition in matured cement paste samples, Mater. Charact. 123 (2017) 294-306.

[11] C.C. Yang, On the relationship between pore structure and chloride diffusivity from accelerated chloride migration test in cement-based materials, Cem. Concr. Res. 36(7) (2006) 1304-1311.

[12] Y. Su, J. Feng, P. Jin, C. Qian, Influence of bacterial self-healing agent on early age performance of cement-based materials, Constr. Build Mater. 218 (2019) 224-234.

[13] S. Wang, X. Ma, L. He, Z. Zhang, L. Li, Y. Li, High strength inorganic-organic polymer composites (IOPC) manufactured by mold pressing of geopolymers, Construction and Building Materials 198 (2019) 501-511.

[14] Q. Ren, Z. Zeng, Z. Jiang, Q. Chen, Incorporation of bamboo charcoal for cement-based humidity adsorption material, Constr. Build Mater. 215 (2019) 244-251.

[15] A.J. Allen, J.J. Thomas, Analysis of C–S–H gel and cement paste by small-angle neutron scattering, Cem. Concr. Res. 37(3) (2007) 319-324.

[16] N. Li, L. Xu, R. Wang, L. Li, P. Wang, Experimental study of calcium sulfoaluminate cement-based self-leveling

compound exposed to various temperatures and moisture conditions: Hydration mechanism and mortar properties, Cem. Concr. Res. 108 (2018) 103-115.

[17] E. Gallucci, K. Scrivener, A. Groso, M. Stampanoni, G. Margaritondo, 3D experimental investigation of the microstructure of cement pastes using synchrotron X-ray microtomography (μCT), Cem. Concr. Res. 37(3) (2007) 360-368.

[18] N. Bossa, P. Chaurand, J. Vicente, D. Borschneck, C. Levard, O. Aguerre-Chariol, J. Rose, Micro- and nano-X-ray computed-tomography: A step forward in the characterization of the pore network of a leached cement paste, Cem. Concr. Res. 67 (2015) 138-147.

[19] M. Zhang, Y. He, G. Ye, D.A. Lange, K.v. Breugel, Computational investigation on mass diffusivity in Portland cement paste based on X-ray computed microtomography (μCT) image, Constr. Build Mater. 27(1) (2012) 472-481.

[20] A. Zankel, J. Wagner, P. Poelt, Serial sectioning methods for 3D investigations in materials science, Micron 62 (2014) 66-78.

[21] B. Chen, M. Yusuf, T. Hashimoto, A.K. Estandarte, G. Thompson, I. Robinson, Three-dimensional positioning and structure of chromosomes in a human prophase nucleus, Sci. adv. 3(7) (2017) e1602231

[22] H. Reingruber, A. Zankel, C. Mayrhofer, P. Poelt, Quantitative characterization of microfiltration membranes by 3D reconstruction, J. Membrane Sci. 372(1-2) (2011) 66-74.

[23] V. Ageh, D. Choudhuri, T.W. Scharf, High frequency reciprocating sliding wear behavior and mechanisms of quaternary metal oxide coatings, Wear 330-331 (2015) 390-399.

[24] A. Trueman, S. Knight, J. Colwell, T. Hashimoto, J. Carr, P. Skeldon, G. Thompson, 3-D tomography by automated in situ block face ultramicrotome imaging using an FEG-SEM to study complex corrosion protective paint coatings, Corros. Sci. 75 (2013) 376-385.

[25] B. Chen, M. Guizar-Sicairos, G. Xiong, L. Shemilt, A. Diaz, J. Nutter, N. Burdet, S. Huo, J. Mancuso, A. Monteith, F. Vergeer, A. Burgess, I. Robinson, Three-dimensional structure analysis and percolation properties of a barrier marine coating, Sci. Rep. 3 (2013) 1177.

[26] S. Busse, T. Hornschemeyer, C. Fischer, Three-dimensional reconstruction on cell level: case study elucidates the ultrastructure of the spinning apparatus of Embia sp. (Insecta: Embioptera), Roy. Soc. Open Sci. 3(10) (2016) 160563.

[27] K. Mukherjee, H.R. Clark, V. Chavan, E.K. Benson, G.J. Kidd, S. Srivastava, Analysis of Brain Mitochondria Using Serial Block-Face Scanning Electron Microscopy, Jove-J. Vis. Exp. (113) (2016) e54214.

[28] P. Wang, N. Li, L. Xu, Hydration evolution and compressive strength of calcium sulphoaluminate cement constantly cured over the temperature range of 0 to 80 °C, Cem. Concr. Res. 100 (2017) 203-213.

[29] S. Borrett, L. Hughes, Reporting methods for processing and analysis of data from serial block face scanning electron microscopy, J. Microsc-Oxford 263(1) (2016) 3-9.

[30] M. Kittelmann, C. Hawes, L. Hughes, Serial block face scanning electron microscopy and the reconstruction of plant cell membrane systems, J. Microsc-Oxford 263(2) (2016) 200-211.

[31] B. Titze, C. Genoud, Volume scanning electron microscopy for imaging biological ultrastructure, Biol. Cell 108(11) (2016) 307-323.

[32] W. Denk, H. Horstmann, Serial block-face scanning electron microscopy to reconstruct three-dimensional tissue nanostructure, Plos Biol. 2(11) (2004) e329.

[33]C.A. Schneider, W.S. Rasband, K.W. Eliceiri, NIH Image to ImageJ: 25 years of image analysis, Nat. methods 9(7) (2012) 671-675.

[34] X. Feng, E.J. Garboczi, D.P. Bentz, P.E. Stutzman, T.O. Mason, Estimation of the degree of hydration of blended cement pastes by a scanning electron microscope point-counting procedure, Cem. Concr. Res. 34(10) (2004) 1787-

1793.
[35] J. Jain, N. Neithalath, Analysis of calcium leaching behavior of plain and modified cement pastes in pure water, Cem. .Concr. Com. 31(3) (2009) 176-185.
[36] W. Sha, E. O'Neill, Z. Guo, Differential scanning calorimetry study of ordinary Portland cement, Cem. Concr. Res. 29(9) (1999) 1487-1489.
[37] A. Wang, C. Zhang, W. Sun, Fly ash effects - II. The active effect of fly ash, Cem. Concr. Res. 34(11) (2004) 2057-2060.
[38] Z. Wu, H. Lian, High performance concrete[M], China Railway Publishing House, 1990.